Biointerface Research in Applied Chemistry
Platinum Open Access Journal (ISSN: 2069-5837)

Article
Volume 12, Issue 3, 2022, 3780 - 3789
https://doi.org/10.33263/BRIAC123.37803789

Molecular Dynamic and Docking Simulation to Prevent Thymine Dimer as the Main Reason for Skin Cancer

Fatemeh Mollaamin [1], Fatma Kandemirli [2], Majid Monajjemi [1,*]

[1] Department of Chemical engineering, Central Tehran Branch, Islamic Azad University, Tehran, Iran
[2] Department of Biomedical Engineering, Faculty of Engineering and Architecture, Kastamonu University, Kastamonu, Turkey
* Correspondence: m_monajjemi@srbiau.ac.ir; maj.monajjemi@iauctb.ac.ir (M.M.);

Scopus Author ID 670181068
Received: 7.04.2021; Revised: 10.05.2021; Accepted: 15.05.2021; Published: 13.08.2021

Abstract: Two major types can be repaired UV-induced DNA lesions. The first one is a light-dependent process that reverts UV damage applying particular wavelengths. The second is a light-independent process that excises the light-damaged region under novo synthesis of an intact DNA. The iGEMDOCK has been used for this study, and the acceptable thymine dimer can be defined for the binding site in whole DNA structures. The DNA is worked with two thymine in a segment of nucleic acids, and iGEMDOCK can help to prepare a suitable binding between them. The total energies of the model systems are a total of several partial energies as follows: $E_{(system)} = E_{(bond)} + E_{(angle)} + E_{(torsion)} + E_{(over)} + E_{(vdW)} + E_{(Coulomb)} + E_{(Specific)}$. $E_{vdW} + E_{(Coulomb)}$ represents the dispersive and electrostatic energies contribution between all atoms, respectively. Finally, $E_{(Specific)}$ is system-specific energy such as lone-pair, conjugation, and hydrogen binding. The DFT and HF calculations of the thymine dimer exhibited that the ring fusion at the C5 and C6 atoms of two thymine bases produced a four-member cyclo-butane puckered ring, as well as the feature, is seen with the MP_n or Moller-Pleset level. In addition, the UV radiations between 360 nm to 200 nm have been investigated for the study of thymine dimers.

Keywords: Molecular dynamic; Docking simulation; thymine dimer; UV radiations

1. Introduction

DNA destroy by ultraviolet (UV) radiations are the main factor contributing to the development of skin cancer. Basically, using antioxidants has been predicated as a protective way against UV-induced skin cancer and is generally frequent in sun places. DNA destroy been done because of direct absorbance of UV, and indirect DNA damaging due to contributed by reactive oxygen species may lead to mutations, resulting in UV-induced skin cancer [1-5]. Two mentioned effects together, and ultraviolet (UV) exposure is the main reason for skin cancer. UV radiation causes the progress of squamous cell carcinoma (SCC) and its precursor lesions, while epidemiologic information indicates the UV radiation as the main reason for the etiology of melanoma and basal cell carcinoma [2,3]. The union of health introduced UV rays as a reason for skin cancer due to the most common form of cancer in nearly half of all cancers [3,4]. Melanoma is the most serious kind of skin cancer as the most general cancer found in young adults. The sun produces 3 types of UV, consisting of UVC, UVB, and UVA that UVA can pass from the ozone layers, making a strong problem in the Earth's atmosphere [5,6]. These UVs penetrate deeper into the skin and are the majority reason for tanning. The genotoxic phenomenon of sunlight's UV (UVA: 325–410 nm and UVB: 290–310 nm) has been

considered for scientists. UV-damages are processed through light-dependent depending on the growth conditions, allowing efficient maintenance of genome integrity[7-9]. UV makes a double bond for forming among the thymine bases in the DNA of skin cells. A strand may appear something like this: G-C-G-C-T-C-T-T-G. When the skin is exposed to UV, the two thymine will bond together, called a thymine dimer [10-14]. To better understand the situation of dimer-mutation and cell lethality and how dimers are distinguished by repairing enzymes, it will be necessary to know how the DNA structure is altered by dimer or by other nucleotide diadducts. X-ray crystallography has been a suitable tool in determining the structures of pyrimidine dimer, psoralen, and cisplatin adducts in dinucleotide forms[15,16]. However, it has not been possible to solve oligonucleotides structures containing these adducts without suitable crystals[17-20]. Other methods such as melting temperature determinations, analysis of randomly damaged DNA on band-counting gels, molecular graphics based on energy minimization combined with model building, and more recently, two-dimensional NMR studies with a dimer-containing dodeca nucleotide has provided some useful, but at times contradictory, information regarding the structure of dimer-containing DNA [20-23].

1.1. Effect of UV on DNA.

DNA, as genetic data, is the main goal of UV due to nucleotides absorption in the range from 105 to 285 nm (UV-C) and from 285 to 310 nm (UV-B) [24-26]. These wavelengths raise nucleotides bases to reactive singlet or triplet states, undergo different photochemical behaviors. Three main types of DNA lesions that appear via these reactions contain two pyrimidine bases and their isomers (Figure 1).

1.2. Photolesion repair mechanism.

Two major types can be repaired UV-induced DNA lesions (Figure 1). The first one is a light-dependent process that reverts UV damage applying particular wavelengths. The second is a light-independent process that excises the light-damaged region under novo synthesis of an intact DNA.

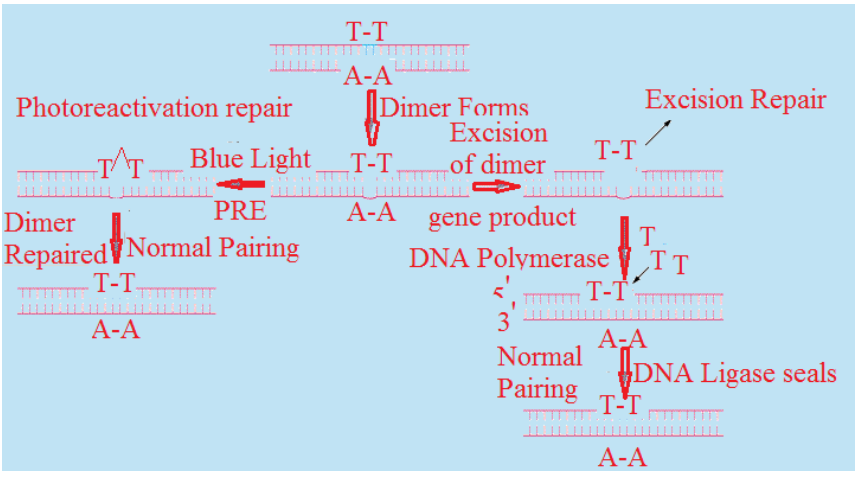

Figure 1. The two different types of DNA repairing for UV radiation damage include UV Base Excision Repair and Photoreactivation.

Although most organisms possess obey of both roots, the light repair pathway is predominantly used. Obviously, growth conditions, tissue specificities, and the transcriptional level of especial genomic area are examples of factors that could define one or the other roots [27-29].

1.3. Light repair.

A necessary repairing root of photon-induced damage(PIR) is a straight repairing that, completely, is based on photon-triggered enzymes or photolysis (Figure 2). In other words, repairing roots does not rely on de novo DNA synthesis. According to phylogenetic analyses, it was assumed that 4 billion years ago, all living organisms possessed photolysis-like genes. DNA photolysis genes appear in all sections of the cell, including eukaryotes. In contrast to its largest sequence and structure similarity, photolysis in DNA repair activity is distinct from cryptochromes that gained new functions as a light receptor, including in the regulation of phototaxis [28-31]. Tight and concentrated focus in a few model organisms such as *E. coli*, *D. melanogaster*, *A. thaliana*, and *S. cerevisiae*, allowed deciphering the specificities of their function. Interestingly, repair activities were recently identified of an N-terminal dinucleotide binding domain and a C-terminal binding domain for the catalytic cofactor: flavin adenine dinucleotide.

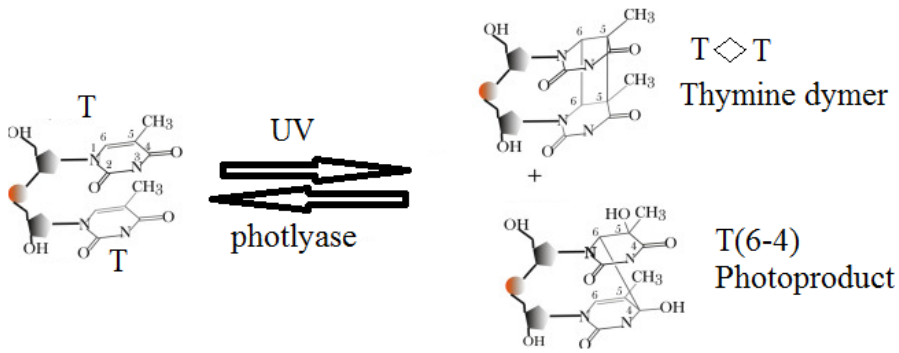

Figure 2. DNA Repairing by photolyase.

1.4. Methylation.

For eukaryotic cells, DNAs are completely packaged into chromatin fiber. The smallest units of chromatin are the nucleosomes, combined with around 150 base pairs DNA attaching to histones, making a platform to regulate gene expression amongst processes, higher chromatin structure, and DNA repair. Notably, the methylation appears at C5 of cytosine as an important epigenetic mark regulating gene expression.

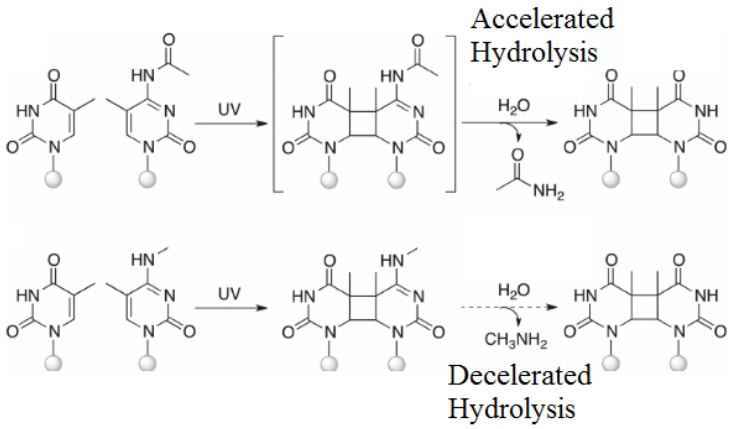

Figure 3. Formation of cyclobutane thymine-cytosine dimers.

The images of photo lesions exhibited that upon UV-R, CPDs are formed around the core histone and in the linker DNA sequence, while 6-4PP is preferentially formed in the linker

region of chromatin [32-35]. It is wonderful that, because of the anisotropic bending preferences of the DNA, the more exposed sequences tend to be enriched in G and C, while the sequences close to the histone core tend to be enriched in A and T. Accelerated and decelerated hydrolysis are shown in Figure 3.

2. Materials and Methods

2.1. Docking analysis.

The iGEMDOCK has been used for this study, and the acceptable thymine dimer can be defined for the binding site in whole DNA structures. The DNA is worked with two thymine in a segment of nucleic acids, and iGEMDOCK can help to prepare a suitable binding between them. Following steps have been accomplished in our modeling: (a), Provide the binding location of thymine dimer on the DNA. (b) Browsing and selecting the DNA-thymine file. (c) Defining the thymine dimers in DNA. (d) Defining the location of the binding by selected nucleotides. (e) Setting the size of the binding site through the extended radius from the selected nucleotides. IGEMDOCK yields an analysis surrounding visualized images and post-analysis for researchers. The minimum energy poses of each system will be outputted into the location of "best: Pose". These analysis data are based on the analysis of those poses. Via looking for the bounded structures of some thymine dimers, it can be selected via the check box of DNA. IGEMDOCK clusters the Thymine dimer based on interaction and atomic composition features. Interaction feature is extracted from the Thymine-Thymine interactions, and atomic composition is accounted atomic types in different functional groups.

2.2. Simulation methodology.

The thymine-thymine dimers interactions are explained via Lennard–Jones potentials as follows: $V_{LJ}(r_{ij}) = 4\varepsilon_{ij}\{[\left(\frac{\sigma_{ij}}{r_{ij}}\right)^{12} - \left(\frac{\sigma_{ij}}{r_{ij}}\right)^{6}]\}, r < R_C$ **(8),** $R_C$is a cutoff distance around 12 Å for VE. In addition, the Lorentz–Berthelot rules have been applied for the inter forces among VE and graphene atoms as follows "$\sigma_{ij} = 0.5(\sigma_i + \sigma_j)"and\ \varepsilon_{ij} = \sqrt{\varepsilon_i} * \sqrt{\varepsilon_j}$. **(9)**. The total energies of the model systems are a total of several partial energies as follows: $E_{(system)}$ = $E_{(bond)}$ + $E_{(angle)}$ + $E_{(torsion)}$ +$E_{(over)}$ +$E_{(vdW)}$ + $E_{(Coulomb)}$ + $E_{(Specific)}$, **(10),** where $E_{(bond)}$ and ($E_{(angle)}$ + $E_{(torsion)}$) are bond formation and angle (both strain and torsional) energies, respectively. $E_{(over)}$ is associated with valence and torsional angles, respectively, that prevent the over-coordination of the atoms. E_{vdW} +$E_{(Coulomb)}$ are the dispersive and electrostatic energies contribution between all atoms, respectively. Finally, $E_{(Specific)}$ is system-specific energy such as lone-pair, conjugation, and hydrogen binding (Tables1&2).

Table 1. Non-bonded parameters in terms of $E_{(van\ der\ waals)}$ + $E_{(Coulomb)}$.

Non bonded interaction

$$V_{LJ}(r_{ij}) = 4\varepsilon_{ij}\{[\left(\frac{\sigma_{ij}}{r_{ij}}\right)^{12} - \left(\frac{\sigma_{ij}}{r_{ij}}\right)^{6}]\}, r < R_C$$

Atom type	**Mass(g/mol)**	$\boldsymbol{\sigma(nm)}$	$\boldsymbol{\varepsilon(\frac{kcal}{mol})}$
N1-N1	28.03	1.78	0.4212
C=O	28.05	3.05	0.16
O-H	17.07	1.22	0.34
C-O	28.05	1.42	0.16
C-C	24.05	2. 23	0.67
N-C	26.04	0.85	0.55

Table 2. Parameters of bonded interactions of the atomistic force field.

Bonded & angle interaction

$$\{[V_b(r_{ij}) = \sum_{bonds} k_{ij}^b (r_{ij} - b_{ij})^2]\} + \{[V_\beta(\theta_{ijk}) = 0.5 \sum_{angle} k_{ijk}^\theta (\theta_{ijk} - \theta_{ijk}^0)^2]\} + \{[V(\varphi_{ijkl}) k_\varphi (1 + Cos(n\varphi - \delta)$$

bond	b(Å)	k^b kcal/mol*Å^2	angle	θ_{ijk}^0	k_{ijk}^θ $(\frac{\text{kcal}}{mol} * Rad^2)$	Dihedral φ_{ijkl}	k_φ kcal/mol	n	δ
C-H	1.15	310	C-O-C	118.5	53.5	C-C-C-O	0.35	1	0.00
C=O	1.20	230	C-C-C	121.0	61.0	H-C-C-C	0.48	3	180.0
O-H	1.08	435	O-C-O	115.5	45.0	O-C-C-H	0.30	2	180.0
C-O	1.40	150	C-C-H	112.4	50.5	C-O-C-H	0.65	2	0.00
C-C	1.51	330	H-C-H	110.4	61.5	H-C-C-H	0.35	1	180.0
C=C	1.35	315	O-C-H	105.2	45.5	O-C-C-O	0.60	3	0.00

The TIP3 is used for a total of the three sites for the electrostatic interactions. The OPLS is a modified form of TIPS that have fitted to liquid state properties. The model works well for various alcohols, amines, aliphatic and aromatic hydrocarbons, sulfur compounds, ether, amino acids, and nucleic acid bases. The OPLS Lennard-Jones parameters for nucleic acid bases are included in Table 3.

Table 3. OPLS Lennard-Jones parameters for nucleic acid bases.

Atom	σ(Å)	$\varepsilon, kcal/mol$
O	1.68	0.343
N	2.87	0.213
C in C=O	3.8	0.220
C normal	3.4	0.122
H(N)	0.0	0.0
H(C)	2.33	0.0
H(O)	1.05	0.0

In the second section of our research, calculations were performed with the simulation program CHARMM in which an empirical energy function, contains two terms of internal and external interactions were used. All modeling and simulation details have been done based on our previous works [36-53].

3. Results and Discussion

The complex structures of 1rys and 1skw (Figure 4) are predicted through dockings modeling and calculated via docking and CHARMM software. The interaction energy analysis indicated the hydrophobic and hydrophilic contributions of related nucleic acids to the Gibbs free energies required for the complex formations. Some of the charged residues exhibited a large unfavorable depending on non-solvation interactions that were canceled out by large favorable columbic interaction, resulting in destabilizing the structures. The free energies of destabilizations are compensated by the van der Waals interactions contemplated by hydrophobic amino acids for giving the stabilizing complexes. Since DNA absorbs wavelengths in the lower part of the UVB band, UV increases the thymine dimer band stronger. Overall, thymine dimer formation in the diatom of human skin on DNA is mainly induced by wavelengths below 320 nm. The free energy differences between two states 1 and 2 of a system can be derived from classical statistical mechanics allowing us to express this function as:

$$A_2 - A_1 = -RTln < \exp\left[-\frac{E_2 - E_1}{RT}\right] >$$

(E_2 - E_1) is the potential energy differences and the symbol < > indicates an ensemble average. Since the isothermal-isobaric ensemble has been used, Gibbs's free energies have the same

expression. The computed free energies are presented in Table 4. Methylation decreases the hydration-free energy of the bases.

Table 4. Solvation free energies.

Method	Adenine	Guanine	Cytosine	Thymine
OPLS,TIP3	-38.44	-45.88	-40.24	-41.2
Charmm	-33.23	-33.47	-31.2	-33.3
OPLF/FEP	-11.8	-22.1	-23.1	-14.1
Amber/FEP	-12.6	-18.9	-13.1	-9.33
Amber/TI	-12.4	-22.1	-17.99	-11.89
AM1/SM2	-19.33	-24.5	-18.55	-13.22
QM/MM	-5.9	-12.9	-16.33	-8.44
SCRF(6-31g*)	-6.11	-16.3	-13.44	-8.45
FDPB	-10.3	-18.8	-16.45	-10.32

The DFT and HF calculations of the thymine dimer exhibited that the ring fusion at the C5 and C6 atoms of two thymine bases produced a four-member cyclo-butane puckered ring, as well as the feature, is seen with the MP_n or Moller-Pleset level. This puckering leads to axial or equatorial positions for the replaced atoms on this ring, and the atoms on the two thymine bases differ in their orientations (Particular in the orientation of the H6A atom). The highest occupied molecular orbital (HOMO) of the neutral T<>T is localized on the C6A-C6B bond. After ionization, the SOMO orbital of TTp-1 is localized on the C6A-C6B bond, and the bond is lengthened compared to the neutral species, as the bond is now weaker due to the single electron occupancy. This 4-member is puckered, as in the neutral forms. The relative orientations of the H6A atom in TTp-1 are the same as the neutral T<>T. Electrons on the C6A-H6A bond participate in the stabilization of the π system. The puckering of the cyclo-butane ring is responsible for the difference in the electronic configuration in the two thymine rings and makes a major order in producing the dissociation path in the thymine dimer. The UV radiations between 360 nm to 200 nm have been investigated for the study of thymine dimers. The small-term in the UVA band (360nm) corresponds with the action spectrum for skin cancer induction. Growth reductions of human cells were also most pronounced in the UVB region. Therefore similarity between wavelength-dependent growth rate reduction and thymine dimer formation was high, especially in the region below 310 nm.

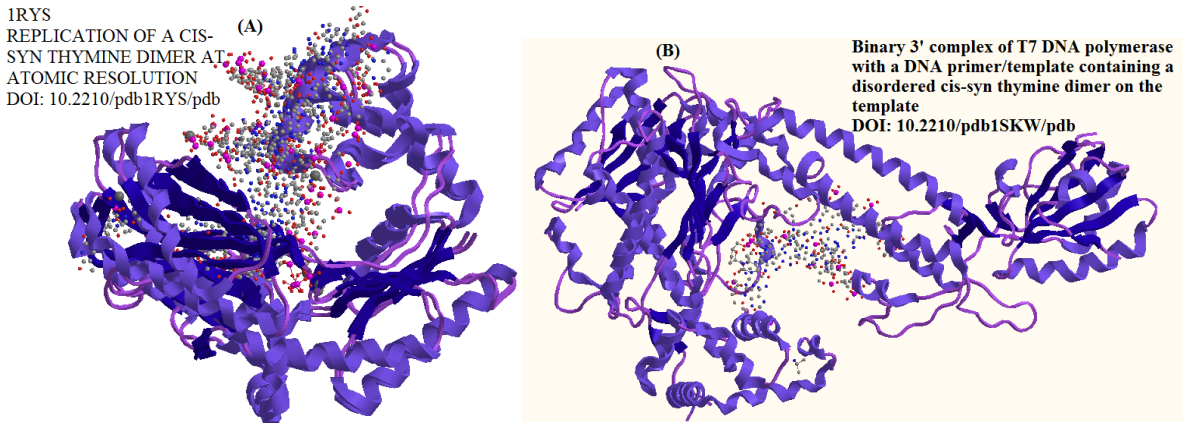

Figure 4. (**A**) Replication of a cis-syn thymine dimer; (**B**) Binary 3' complex of T7 DNA polymerase with a DNA primer/template containing a disordered cis-syn thymine dimer.

The overall similarity suggests that growth inhibition can be explained by thymine dimer formation combined with an insufficient repair. Since photo repair of thymine dimers is

induced by wavelengths between 310 and 400 nm, the ratio between UVB, UVA, and PAR determines whether damage and repair are in balance. In the light of this notion, growth rate reduction in the UVB region was caused by the unbalance between thymine dimer formation and repair [54-67].

4. Conclusions

The DFT and HF calculations of the thymine dimer exhibited that the ring fusion at the C5 and C6 atoms of two thymine bases produced a four-member cyclo-butane puckered ring, as well, as the feature is seen with the MP_n or Moller-Pleset level. Since photo repair of thymine dimers is induced by wavelengths between 310 and 400 nm, the ratio between UVB, UVA, and PAR determines whether damage and repair are in balance.

Funding

This research received no external funding.

Acknowledgments

The Authors thanks both universities: Kastamonu University & Islamic Azad University for providing computer equipment and software

Conflicts of Interest

The authors declare no conflict of interest.

References

1. Hodges, A.J.; Plummer, D.A.; Wyrick, J.J. NuA4 acetyltransferase is required for efficient nucleotide excision repair in yeast. *DNA Repair* **2019**, *73*, 91–98, https://doi.org/10.1016/j.dnarep.2018.11.006.
2. Schick, S.; Fournier, D.; Thakurela, S.; Sahu, S.K.; Garding, A.; Tiwari, V.K. Dynamics of chromatin accessibility and epigenetic state in response to UV damage. *J. Cell. Sci.* **2015**, *128*, 4380–4394, https://doi.org/10.1242/jcs.173633.
3. Ferrand, J.; Plessier, A.; Polo, S.E. Control of the chromatin response to DNA damage: Histone proteins pull the strings. *Semin. Cell Dev. Biol.* **2020**, https://doi.org/10.1016/j.semcdb.2020.07.002.
4. Wang, J.; Li, X.; Do Kim, K.; Scanlon, M.J.; Jackson, S.A.; Springer, N.M.; Yu, J. Genome-wide nucleotide patterns and potential mechanisms of genome divergence following domestication in maize and soybean. *Genome Biol.* **2019**, *20*, 74, https://doi.org/10.1186/s13059-019-1683-6.
5. Rimel, J.K.; Taatjes, D.J. The essential and multifunctional TFIIH complex. *Protein Sci.* **2018**, *27*, 1018–1037, https://doi.org/10.1002/pro.3424.
6. Greber, B.J.; Toso, D.B.; Fang, J.; Nogales, E. The complete structure of the human TFIIH core complex. *Elife* **2019**, *8*, https://doi.org/10.7554/eLife.44771.
7. Liu, L.; Huo, Y.; Li, J.; Jiang, T. Crystal structure of the yeast Rad7-Elc1 complex and assembly of the Rad7-Rad16-Elc1-Cul3 complex. *DNA Repair* **2019**, *77*, 1–9, https://doi.org/10.1016/j.dnarep.2019.02.012.
8. Lahari, T.; Lazaro, J.; Marcus, J.M.; Schroeder, D.F. RAD7 homologues contribute to Arabidopsis UV tolerance. *Plant Sci.* **2018**, *277*, 267–277, https://doi.org/10.1016/j.plantsci.2018.09.017.
9. Kumar, R.; Sabapathy, K. RNF4-A Paradigm for SUMOylation-Mediated Ubiquitination. *Proteomics* **2019**, *19*, e1900185, https://doi.org/10.1002/pmic.201900185.
10. Rüthemann, P.; Balbo Pogliano, C.; Codilupi, T.; Garajovà, Z.; Naegeli, H. Chromatin remodeler CHD1 promotes XPC-to-TFIIH handover of nucleosomal UV lesions in nucleotide excision repair. *EMBO J.* **2017**, *36*, 3372–3386, https://doi.org/10.15252/embj.201695742.
11. Jang, S.; Kumar, N.; Beckwitt, E.C.; Kong, M.; Fouquerel, E.; Rapi'c-Otrin, V.; Prasad, R.; Watkins, S.C.; Khuu, C.; Majumdar, C.; David, S.S.; Wilson, S.H.; Bruchez, M.P.; Opresko, P.L.; Van Houten, B. Damage

sensor role of UV-DDB during base excision repair. *Nat. Struct. Mol. Biol.* **2019**, *26*, 695–703, https://doi.org/10.1038/s41594-019-0261-7.
12. Borgermann, N.; Ackermann, L.; Schwertman, P.; Hendriks, I.A.; Thijssen, K.; Liu, J.C.; Lans, H.; Nielsen, M.L.; Mailand, N. SUMOylation promotes protective responses to DNA-protein crosslinks. *EMBO J.* **2019**, *38*, https://doi.org/10.15252/embj.2019101496.
13. Balbo Pogliano, C.; Gatti, M.; Rüthemann, P.; Garajovà, Z.; Penengo, L.; Naegeli, H. ASH1L histone methyltransferase regulates the handoff between damage recognition factors in global-genome nucleotide excision repair. *Nat. Commun.* **2017**, *8*, https://doi.org/10.1038/s41467-017-01080-8.
14. Zhu, B.; Chen, S.; Wang, H.; Yin, C.; Han, C.; Peng, C.; Liu, Z.; Wan, L.; Zhang, X.; Zhang, J.; Lian, CG.; Ma, P.; Xu, Z.X.; Prince, S.; Wang, T.; Gao, X.; Shi, Y.; Liu, D.; Liu, M.; Wei, W.; Wei, Z.; Pan, J.; Wang, Y.; Xuan, Z.; Hess, J.; Hayward, N.K.; Goding, C.R.; Chen, X.; Zhou, J.; Cui, R. The protective role of DOT1L in UV-induced melanomagenesis. *Nat. Commun.* **2018**, *9*, 259, https://doi.org/10.1038/s41467-017-02687-7.
15. Chitale, S.; Richly, H. DICER- and MMSET-catalyzed H4K20me2 recruits the nucleotide excision repair factor XPA to DNA damage sites. *J. Cell Biol.* **2018**, *217*, 527–540, https://doi.org/10.1083/jcb.201704028.
16. Gsell, C.; Richly, H.; Coin, F.; Naegeli, H. A chromatin scaffold for DNA damage recognition: How histone methyltransferases prime nucleosomes for repair of ultraviolet light-induced lesions. *Nucleic Acids Res.* **2020**, *48*, 1652–1668, https://doi.org/10.1093/nar/gkz1229.
17. Panigrahi, A.; Vemuri, H.; Aggarwal, M.; Pitta, K.; Krishnan, M. Sequence specificity, energetics and mechanism of mismatch recognition by DNA damage sensing protein Rad4/XPC. *Nucleic Acids Res.* **2020**, *48*, 2246–2257, https://doi.org/10.1093/nar/gkaa078.
18. Matsumoto, S.; Cavadini, S.; Bunker, R.D.; Grand, R.S.; Potenza, A.; Rabl, J.; Yamamoto, J.; Schenk, A.D.; Schübeler, D.; Iwai, S.; Sugasawa, K.; Kurumizaka, H.; Thoma, N.H. DNA damage detection in nucleosomes involves DNA register shifting. *Nature* **2019**, *571*, 79–84, https://doi.org/10.1038/s41586-019-1259-3.
19. Paul, D.; Mu, H.; Zhao, H.; Ouerfelli, O.; Jeffrey, P.D.; Broyde, S.; Min, J.-H. Structure and mechanism of pyrimidine-pyrimidone (6-4) photoproduct recognition by the Rad4/XPC nucleotide excision repair complex. *Nucleic Acids Res.* **2019**, *47*, 6015–6028, https://doi.org/10.1093/nar/gkz359.
20. Kokic, G.; Chernev, A.; Tegunov, D.; Dienemann, C.; Urlaub, H.; Cramer, P. Structural basis of TFIIH activation for nucleotide excision repair. *Nat. Commun.* **2019**, *10*, 2885, https://doi.org/10.1038/s41467-019-10745-5.
21. Daniel, L.; Cerutti, E.; Donnio, L.-M.; Nonnekens, J.; Carrat, C.; Zahova, S.; Mari, P.-O.; Giglia-Mari, G. Mechanistic insights in transcription-coupled nucleotide excision repair of ribosomal DNA. *Proc. Natl. Acad. Sci. USA* **2018**, *115*, E6770–E6779, https://doi.org/10.1073/pnas.1716581115.
22. Willis, I.M.; Moir, R.D. Signaling to and from the RNA Polymerase III Transcription and Processing Machinery. *Annu. Rev. Biochem.* **2018**, *87*, 75–100, https://doi.org/10.1146/annurev-biochem-062917-012624.
23. Sanz-Murillo, M.; Xu, J.; Belogurov, G.A.; Calvo, O.; Gil-Carton, D.; Moreno-Morcillo, M.; Wang, D.; Fernández-Tornero, C. Structural basis of RNA polymerase I stalling at UV light-induced DNA damage. *Proc. Natl. Acad. Sci. USA* **2018**, *115*, 8972–8977, https://doi.org/10.1073/pnas.1802626115.
24. Le, T.T.; Yang, Y.; Tan, C.; Suhanovsky, M.M.; Fulbright, R.M.; Inman, J.T.; Li, M.; Lee, J.; Perelman, S.; Roberts, J.W.; Deaconescu, A.M.; Wang, M.D. Mfd Dynamically Regulates Transcription via a Release and Catch-Up Mechanism. *Cell* **2018**, *172*, 344–357.e15, https://doi.org/10.1016/j.cell.2018.06.002.
25. Selby, C.P. Mfd Protein and Transcription-Repair Coupling in Escherichia coli. *Photochem. Photobiol.* **2017**, *93*, 280–295, https://doi.org/10.1111/php.12675.
26. Al Khateeb, W.M.; Sher, A.A.; Marcus, J.M.; Schroeder, D.F. UVSSA, UBP12, and RDO2/TFIIS Contribute to Arabidopsis UV Tolerance. *Front. Plant Sci.* **2019**, *10*, https://doi.org/10.3389/fpls.2019.00516.
27. Deger, N.; Yang, Y.; Lindsey-Boltz, L.A.; Sancar, A.; Selby, C.P. Drosophila, which lacks canonical transcription-coupled repair proteins, performs transcription-coupled repair. *J. Biol. Chem.* **2019**, *294*, 18092–18098, https://doi.org/10.1074/jbc.AC119.011448.
28. Liebelt, F.; Schimmel, J.; Verlaan- de Vries, M.; Klemann, E.; van Royen, M.E.; van der Weegen, Y.; Luijsterburg, M.S.; Mullenders, L.H.; Pines, A.; Vermeulen, W.; Vertegaal, A.C.O. Transcription-coupled nucleotide excision repair is coordinated by ubiquitin and SUMO in response to ultraviolet irradiation. *Nucleic Acids Res.* **2020**, *48*, 231–248, https://doi.org/10.1093/nar/gkz977.
29. van der Weegen, Y.; Golan-Berman, H.; Mevissen, T.E.T.; Apelt, K.; González-Prieto, R.; Goedhart, J.; Heilbrun, E.E.; Vertegaal, A.C.O.; van den Heuvel, D.; Walter, J.C.; Adar, S.; Luijsterburg, M.S. The

cooperative action of CSB, CSA, and UVSSA target TFIIH to DNA damage-stalled RNA polymerase II. *Nat. Commun.* **2020**, *11*, https://doi.org/10.1038/s41467-020-15903-8.
30. Mullenders, L. DNA damage mediated transcription arrest: Step back to go forward. *Dna Repair* **2015**, *36*, 28–35, https://doi.org/10.1016/j.dnarep.2015.09.005.
31. Lans, H.; Hoeijmakers, J.H.J.; Vermeulen, W.; Marteijn, J.A. The DNA damage response to transcription stress. *Nat. Rev. Mol. Cell Biol.* **2019**, *20*, 766–784, https://doi.org/10.1038/s41580-019-0169-4.
32. Wang, W.; Xu, J.; Chong, J.; Wang, D. Structural Basis of DNA Lesion Recognition for Eukaryotic Transcription-Coupled Nucleotide Excision Repair. *DNA Repair* **2018**, *71*, 43–55, https://doi.org/10.1016/j.dnarep.2018.08.006.
33. Zhu, Q.; Ding, N.; Wei, S.; Li, P.; Wani, G.; He, J.; Wani, A.A. USP7-mediated deubiquitination differentially regulates CSB but not UVSSA upon UV radiation-induced DNA damage. *Cell Cycle* **2020**, *19*, 124–141, https://doi.org/10.1080/15384101.2019.1695996.
34. Nakazawa, Y.; Hara, Y.; Oka, Y.; Komine, O.; van den Heuvel, D.; Guo, C.; Daigaku, Y.; Isono, M.; He, Y.; Shimada, M.; Kato, K.; Jia, N.; Hashimoto, S.; Kotani, Y.; Miyoshi, Y.; Tanaka, M.; Sobue, A.; Mitsutake, N.; Suganami, T.; Masuda, A.; Ohno, K.; Nakada, S.; Mashimo, T.; Yamanaka, K.; Luijsterburg, M.S.; Ogi, T. Ubiquitination of DNA Damage-Stalled RNAPII Promotes Transcription-Coupled Repair. *Cell* **2020**, *180*, 1228–1244, https://doi.org/10.1016/j.cell.2020.02.010.
35. Tufegdžic Vidakovic, A.; Mitter, R.; Kelly, G.P.; Neumann, M.; Harreman, M.; Rodríguez-Martínez, M.; Herlihy, A.; Weems, J.C.; Boeing, S.; Encheva, V.; Gaul, L.; Milligan, L.; Tollervey, D.; Conaway, R.C.; Conaway, J.W.; Snijders, A.P.; Stewart, A.; Svejstrup, J.Q. Regulation of the RNAPII Pool Is Integral to the DNA Damage Response. *Cell* **2020**, *180*, 1245–1261.e21, https://doi.org/10.1016/j.cell.2020.02.009.
36. Monajjemi, M. Cell membrane causes the lipid bilayers to behave as variable capacitors: A resonance with self-induction of helical proteins. *Biophysical Chemistry* **2015**, *207*, 114-127, https://doi.org/10.1016/j.bpc.2015.10.003.
37. Monajjemi, M. Liquid-phase exfoliation (LPE) of graphite towards graphene: An ab initio study. *Journal of Molecular Liquids*, **2017**, *230*, 461–472, https://doi.org/10.1016/j.molliq.2017.01.044.
38. Monajjemi, M.; Naderi, F.; Mollaamin, F.; Khaleghian, M. Drug design outlook by calculation of second virial coefficient as a nano study. *Journal of the Mexican Chemical Society* **2012**, *56*, 207-211, https://doi.org/10.29356/jmcs.v56i2.323.
39. Monajjemi, M.; Bagheri, S.; Moosavi, M.S. Symmetry breaking of B2N(-,0,+): An aspect of the electric potential and atomic charges. *Molecules* **2015**, *20*, 21636-21657, https://doi.org/10.3390/molecules201219769.
40. Monajjemi, M.; Mohammadian, N.T. S-NICS: An aromaticity criterion for nano molecules. *Journal of Computational and Theoretical Nanoscience* **2015**, *12*, 4895-4914, https://doi.org/10.1166/jctn.2015.4458.
41. Monajjemi, M.; Ketabi, S.; Hashemian, Z.M.; Amiri, A. Simulation of DNA bases in water: Comparison of the Monte Carlo algorithm with molecular mechanics force fields. *Biochemistry (Moscow)* **2006**, *71*, 1-8, https://doi.org/10.1134/s0006297906130013.
42. Monajjemi, M.; Lee, V.S.; Khaleghian, M.; Honarparvar, B.; Mollaamin, F. Theoretical Description of Electromagnetic Nonbonded Interactions of Radical, Cationic, and Anionic NH2BHNBHNH2 Inside of the B18N18 Nanoring. *J. Phys. Chem C* **2010**, *114*, 15315-15330, https://doi.org/10.1021/jp104274z.
43. Monajjemi, M.; Boggs, J.E. A New Generation of BnNn Rings as a Supplement to Boron Nitride Tubes and Cages. *J. Phys. Chem. A* **2013**, *117*, 1670-1684, http://dx.doi.org/10.1021/jp312073q.
44. Monajjemi, M. Non bonded interaction between BnNn (stator) and BN B (rotor) systems: A quantum rotation in IR region. *Chemical Physics* **2013**, *425*, 29-45, https://doi.org/10.1016/j.chemphys.2013.07.014.
45. Monajjemi, M.; Robert, W.J.; Boggs, J.E. NMR contour maps as a new parameter of carboxyl's OH groups in amino acids recognition: A reason of tRNA–amino acid conjugation. *Chemical Physics* **2014**, *433*, 1-11, https://doi.org/10.1016/j.chemphys.2014.01.017.
46. Monajjemi, M. Quantum investigation of non-bonded interaction between the B15N15 ring and BH2NBH2 (radical, cation, and anion) systems: a nano molecularmotor. *Struct Chem* **2012,** *23*, 551–580, http://dx.doi.org/10.1007/s11224-011-9895-8.
47. Monajjemi, M. Metal-doped graphene layers composed with boron nitride–graphene as an insulator: a nanocapacitor. *Journal of Molecular Modeling* **2014**, *20*, 2507, https://doi.org/10.1007/s00894-014-2507-y.
48. Monajjemi, M.; Heshmat, M.; Haeri, H.H.; Kaveh, F. Theoretical study of vitamin properties from combined QM-MM methods: Comparison of chemical shifts and energy. *Russian Journal of Physical Chemistry* **2006**, *80*, 1061-1068, https://doi.org/10.1134/S0036024406070119.

49. Monajjemi, M.; Honaparvar, B.; Khalili Hadad, B.; Ilkhani, A.; Mollaamin, F. Thermo-Chemical Investigation and NBO Analysis of Some anxileotic as Nano- Drugs. *African journal of pharmacy and pharmacology* **2010**, *4*, 521-529, https://doi.org/10.5897/AJPP.9000278
50. Monajjemi, M., Najafpour, J., Mollaamin, F. (3,3)4 Armchair carbon nanotube in connection with PNP and NPN junctions: Ab Initio and DFT-based studies. *Fullerenes Nanotubes and Carbon Nanostructures* **2013**, *21*, 213-232, https://doi.org/10.1080/1536383X.2011.597010.
51. Monajjemi, M., Jafari Azan, M., Mollaamin, F. Density functional theory study on B30N20 nanocage in structural properties and thermochemical outlook. *Fullerenes Nanotubes and Carbon Nanostructures* **2013**, *21*, 503-515, https://doi.org/10.1080/1536383X.2011.629762.
52. Monajjemi, M.; Ghiasi, R.; Ketabi, S.; Passdar, H.; Mollaamin, F. A Theoretical Study of Metal-Stabilised Rare Tautomers Stability: N4 Metalated Cytosine (M=Be2+, Mg2+, Ca2+, Sr2+ and Ba2+) in Gas Phase and Different. *Journal of Chemical Research* **2004**, *1*, 11-18, https://doi.org/10.3184/030823404323000648.
53. Monajjemi, M., Baheri, H., Mollaamin, F. A percolation model for carbon nanotube-polymer composites using the Mandelbrot-Given. *Journal of Structural Chemistry* **2011**, *52*, 54-59, https://doi.org/10.1134/S0022476611010070.
54. Maestre-Reyna, M.; Yamamoto, J.; Huang, W.-C.; Tsai, M.-D.; Essen, L.-O.; Bessho, Y. Twist and turn: A revised structural view on the unpaired bubble of class II CPD photolyase in complex with damaged DNA. *IUCrJ* **2018**, *5*, 608–618, https://doi.org/10.1107/S205225251800996X.
55. Marizcurrena, J.J.; Acosta, S.; Canclini, L.; Hernández, P.; Vallés, D.; Lamparter, T.; Castro-Sowinski, S. A natural occurring bifunctional CPD/(6-4)-photolyase from the Antarctic bacterium Sphingomonas sp. UV9. *Appl. Microbiol. Biotechnol.* **2020**, *104*, 7037-7050, https://doi.org/10.1007/s00253-020-10734-5.
56. Vechtomova, Y.L.; Telegina, T.A.; Kritsky, M.S. Evolution of Proteins of the DNA Photolyase/Cryptochrome Family. *Biochem. Mosc.* **2020**, *85*, 131–153, https://doi.org/10.1134/S0006297920140072.
57. Premi, S.; Han, L.; Mehta, S.; Knight, J.; Zhao, D.; Palmatier, M.A.; Kornacker, K.; Brash, D.E. Genomic sites hypersensitive to ultraviolet radiation. *Proc. Natl. Acad. Sci. USA* **2019**, *116*, 24196–24205, https://doi.org/10.1073/pnas.1907860116.
58. Graindorge, S.; Cognat, V.; Johann to Berens, P.; Mutterer, J.; Molinier, J. Photodamage repair pathways contribute to the accurate maintenance of the DNA methylome landscape upon UV exposure. *PLoS Genet.* **2019**, *15*, e1008476, https://doi.org/10.1371/journal.pgen.1008476.
59. Chung, L.H.; Murray, V. An extended sequence specificity for UV-induced DNA damage. *J. Photochem. Photobiol. B Biol.* **2018**, *178*, 133–142, https://doi.org/10.1016/j.jphotobiol.2017.10.034.
60. Douki, T. Pyrimidine (6-4) Pyrimidone Photoproducts in UVA-Irradiated DNA: Photosensitization or Photoisomerization? *ChemPhotoChem* **2020**, *4*, 294–299, https://doi.org/10.1002/cptc.201900280.
61. Marizcurrena, J.J.; Acosta, S.; Canclini, L.; Hernández, P.; Vallés, D.; Lamparter, T.; Castro-Sowinski, S. A natural occurring bifunctional CPD/(6-4)-photolyase from the Antarctic bacterium Sphingomonas sp. UV9. *Appl. Microbiol. Biotechnol.* **2020**, *104*, 7037–7050, https://doi.org/10.1007/s00253-020-10734-5.
62. Strzalka, W.; Zglobicki, P.; Bazant, A.; Kowalska, E.; Dziga, D.; Banas, A.K. The dark side of the UV induced lesions repair. *Genes* **2020**, *11*, https://doi.org/10.3390/genes11121450.
63. Hung, K.F.; Sidorova, J.M.; Nghiem, P.; Kawasumi, M. The 6-4 photoproduct is the trigger of UV-induced replication blockage and ATR activation. *Proc. Natl. Acad. Sci. USA* **2020**, *117*, 12806–12816, https://doi.org/10.1073/pnas.1917196117.
64. Valenta, K.; Dimac-Stohl, K.; Baines, F.; Smith, T.; Piotrowski, G.; Hill, N.; Kuppler, J.; Nevo, O. Ultraviolet radiation changes plant color. *BMC Plant Biol.* **2020**, *20*, 253, https://doi.org/10.1186/s12870-020-02471-8.
65. Wu, E.J.; Wang, Y.P.; Yahuza, L.; He, M.H.; Sun, D.L.; Huang, Y.M.; Liu, Y.C.; Yang, L.N.; Zhu, W.; Zhan, J. Rapid adaptation of the Irish potato famine pathogen *Phytophthora infestans* to changing temperature. *Evol. Appl.* **2020**, *13*, 768–780, https://doi.org/10.1111/eva.12899.
66. Guo, W.; Xin, M.; Wang, Z.; Yao, Y.; Hu, Z.; Song, W.; Yu, K.; Chen, Y.; Wang, X.; Guan, P.; Appels, R.; Peng, H.; Ni, Z.; Sun, Q. Origin and adaptation to high altitude of Tibetan semi-wild wheat. *Nat. Commun.* **2020**, *11*, 5085, https://doi.org/10.1038/s41467-020-18738-5.
67. Karimpour Motlagh, K.N.; Khonakdar, H.A.; Jafari, S.H.; Panahi, S.M.; Javadi, A. ; Shojaei,S.; Godarzi, V, An experimental and theoretical mechanic analysis of thermal degardation of polypropylene/polylactic acid/clay nano particle. *Polymers for advanced Technologies* , **2019**, 30(11), 2695-2706, https://doi.org/10.1002/pat.4699.